Laminar Newtonian flows in square curved ducts at moderate Reynolds number

J. Malheiro[1], P.J. Oliveira[1], F.T. Pinho[2]
[1]Universidade da Beira Interior, [2]Faculdade Engenharia Universidade Porto

Abstract

The present numerical study is an introductory computer simulation work on the characteristics of incompressible fluid flow in curved ducts of square cross section. Here, the fluid is assumed Newtonian and the conditions of Bara *et al* [3], Mees *et al* [4] and Helin *et al* [7] were considered, in order to make comparison of results. Good agreement between the velocity profiles were found, especially for the lower Reynolds number (*Re*) considered. As *Re* was increased to 532 and 583, differences were observed at the end part of the curve. Those differences were higher for *Re*=583 and other solutions were presented to match the results of Bara *et al* [3].

Introduction

Fluid flows in curved ducts can be found in many industrial and engineering applications, such as in most fluid transport systems within the chemical, food and manufacturing industries, in environmental engineering, in waste heat recovery systems, in air-conditioning, refrigeration and power production system ducts and in bio-engineering (e.g., human organs – arteries, lungs, catheter, etc.). Since the early XXth century this type of flow arose a particular interest in the scientific community. This interest comes from the centrifugal induced secondary flows first reported by Dean in 1927 that straight channels do not show. Although this secondary flows may have undesirable effects (e.g., increase in pressure drop; degradation of long chain molecules of polymeric fluids by the high shear stress), it can also be beneficial as it improves heat and mass transfer (e.g., in thermal homogeneity and membrane separation, respectively), enhance cross-sectional mixing (e.g., homogeneity of a mixture along the cross-section of the channel) and reduction in axial dispersion (e.g., diffusion of a solute in a flowing liquid). [1, 2].

The secondary flow in a curved channel, also known as Dean flow, is induced by unbalanced centrifugal forces, as consequence of a non-uniform axial velocity distribution, and results in a pressure gradient normal to the streamwise direction. This pressure gradient (the pressure is higher at the outer wall than at the inner, bottom and top walls, where there is slow moving fluid) generates a secondary flow from the outer to the side and inner walls and finally towards the centre of the channel which then feeds the outer wall region. Thus, the flow is characterized by two symmetrical vortices that occupy the entire cross-section of the channel and its magnitude is measured by the Dean number (*Dn*). The Dean number is defined by the ratio of the square root of the product of inertial and centrifugal forces to the viscous force [3]:

$Dn = \frac{\mathrm{Re}}{\sqrt{Rc}}$, where $\mathrm{Re} = \frac{\rho U a}{\mu}$ is the Reynolds number and $Rc = \frac{R}{a}$ is the curvature ratio [3]. *U* is the average velocity at inlet, *a* is the side of the square cross section and *R* is the radius of curvature of the channel. However, as *Re* is increased, in the laminar regime, the flow becomes more complex and a second symmetrical pair of counter-rotating vortices appears near the outer wall [3]. Mees *et al* [4] showed that at *Dn* = 453 a third pair of counter-rotating vortices appears, Winters [5] presented multiple solutions within certain ranges of values of *Re*, and Soh [6] showed that the inlet conditions affect the flow downstream. More recently, Helin *et al* [7], following the same geometry of Bara *et al* [3], presented results of the development of the flow considering a viscoelastic fluid. Many works dealing with flows in curved channels have been published [1, 2], for different cross-sections, values of *Re* (or *Dn*), curvature ratios, fluid models, etc., using both numerical and experimental approaches, and thus showing how complex this kind of flow can be. However flows in curved channels of complex fluids are not yet completely understood, and even for Newtonian fluids the results obtained by different investigations are not always in agreement thus justifying the present contribution.

Governing Equations

Here we consider three-dimensional, laminar, isothermal, steady flow of an incompressible Newtonian fluid. The governing equations, which describe the behaviour of the flow, are presented in general form:

i) Mass conservation:

$$\nabla . \boldsymbol{u} = 0$$

ii) Momentum conservation:

$$\rho \frac{D\boldsymbol{u}}{Dt} \equiv \rho \frac{\partial \boldsymbol{u}}{\partial t} + \rho \boldsymbol{u}.\nabla \boldsymbol{u} = -\nabla p + \nabla . \boldsymbol{\tau}_{tot}$$

where $\boldsymbol{u}$ is the velocity vector (with *u*, *v* and *w* components for the *x*, *y* and *z* directions, respectively), ρ is the fluid density, *t* is the time, *p* the pressure and $\boldsymbol{\tau}_{\mathrm{tot}}$ the extra stress tensor.

iii) Constitutive equation:

$$\boldsymbol{\tau} = \eta \dot{\boldsymbol{\gamma}} = \eta \left(\nabla \boldsymbol{u} + (\nabla \boldsymbol{u})^T \right) = 2\eta \boldsymbol{D}$$

which is Newton's law for viscosity, where η is the constant fluid viscosity and $(\nabla \boldsymbol{u})^T$ is the transpose of the velocity gradient tensor.

Numerical Method

The numerical solution of the governing equations is obtained by the Finite Volume Method, which maps the computational domain in cells (control volumes) and discretizes the equation in time and space, resulting in a

linearized set of algebraic equations solved by adequate conjugate gradient solvers and the SIMPLEC algorithm.
The geometry is a three-dimensional curved channel with square cross-section. To generate the mesh the channel is divided into three blocks (Figure 1-a)):

i) Block I: a straight channel of width $a=1$ and length $Le=20a$ at the entrance;
ii) Block II: a connecting 180º curved channel, with internal radius $R1=14.6a$ and external radius $R2=15.6a$ (these dimensions are the same as those of Bara *et al* [3], Mees *et al* [4] and Helin *et al* [7] $R=\frac{(R1+R2)}{2}=15.1$);
iii) Block III: and a straight channel at the exit, having the same dimensions as the inlet channel.

The origin of the Cartesian coordinates system (*x*, *y*, *z*) is at the bottom corner of the first block of the curved channel (Figure 1-b)). A non-uniform spaced mesh has been used and its geometrical characteristics are presented in Table 1. This table shows the number of cells in each block for each direction, the total number of control volumes (NCV) and the factor of compression/expansion (*f*) for each direction. The value of this factor defines the size of the smallest cell and is such that guarantees smooth transition between cell dimensions. Thus, when the mesh is uniform it takes the value of one, and when the mesh is non-uniform, as the case here, the compression factor in the *x* direction is about 4.8% in Block I and the expansion factor is about 5% in Block III.

Table 1 – Geometrical characteristics of the computational mesh

	Mesh			
	NX × NY × NZ	f_x	f_y	f_z
Block I	30 × 20 × 20	0.95212	1.00000	1.00000
Block II	161 × 20 × 20	1.00000	1.00000	1.00000
Block III	30 × 20 × 20	1.05029	1.00000	1.00000
NCV	88400			

A no-slip condition is applied at all walls ($u = v = w = 0$) and a uniform velocity profile is imposed at the inlet of the entrance channel. Its length is such as to guarantee that the flow is fully developed when entering the curved part of the channel. At the exit of the outlet channel a zero axial-gradient condition was imposed. The simulations were done using the entire domain of the channel, due to the possibility of occurrence of asymmetries in the flow.

Results and Discussion

The results are presented mainly for three different Re numbers: *Re* = 486, *Re* = 532 and *Re* = 583, which correspond to *Dn* = 125, *Dn* = 137 and *Dn* = 150, respectively. The same conditions from Bara *et al* [3], which were later considered by Mees *et al* [4] and Helin *et al* [7], were also assumed here. Figure 2 exhibits contour and vector plots of the distribution of dimensionless streamwise velocity and the secondary

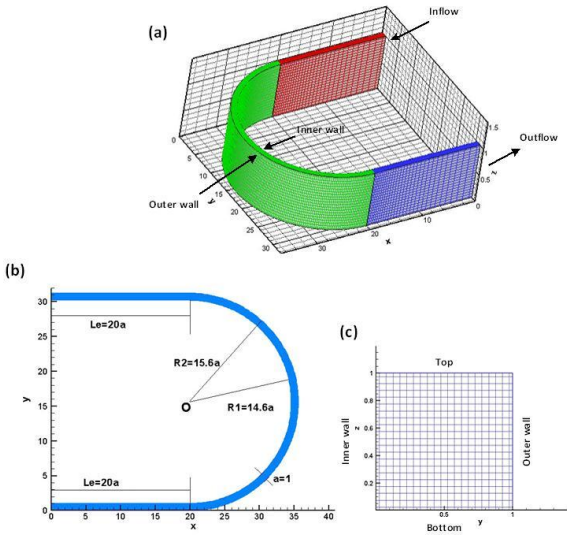

Figure 1 – Geometrical characteristics of the channel (geometry not to scale).

velocity field at the entry to the curve. At this position the maximum of the velocity is located at the centre of the channel, which corresponds approximately to a parabolic velocity profile along the symmetry plane of the cross-section. Theoretically this velocity for fully-developed flow in a straight square duct is 2.096 and numerically we obtained 1.978, 1.959 and 1.939 for *Re* = 486, *Re* = 532 and *Re* = 583 in the curved duct, respectively.

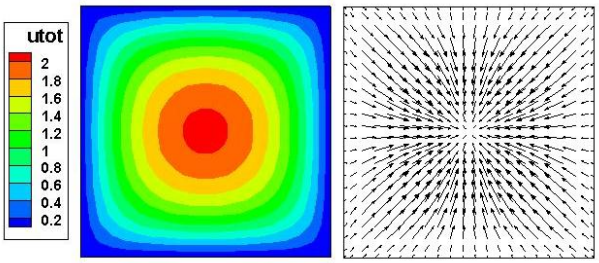

Figure 2 – Contours and vector plots of dimensionless axial and secondary velocity at the entry to the curved channel.

At the beginning of the curve, the flow tends, in the first place, to run as in a straight channel due to its inertia until it finds the outer wall. As the fluid moves along the curve, the centrifugal force maintains the maximum velocity towards the outer wall as illustrated in Figure 3, which shows contours of axial velocity along the curve mid-plane (*z*=0.5) and also axial velocity contours and secondary velocity vector plots in the cross-section at 90º (middle of the curve), for different values of *Re*. This figure demonstrates that, at 90º, the secondary flow is already established and the two symmetrical counter-rotating vortices are clearly observed. Looking to the vector plots in Figure 3, and as shown previously [3,7] at this location of the channel there is still no sign of an additional pair of vortices, except for *Re*=583 which shows, near the outer wall and between the large vortices,

the early development of an additional pair of smaller vortices. This could probably be predicted with a refined mesh near the outer wall

The development of the streamwise velocity profiles along the symmetry plane of the channel is plotted in Figure 4. In this figure the results are compared with those of Bara *et al* [3]. For *Re*= 486, at the beginning of the curve (20º), the velocity profile is already asymmetric and the maximum velocity is located near the outer wall due to the inertia of the incoming flow. At 40º, the maximum velocity has decreased and started to move back to the centre of the channel and the velocity near the inner wall increase, as a result of the redistribution of momentum induced by the secondary flow that is gradually setting in. At 60º the transfer of momentum continues and the velocity near the inner wall and centre slightly increase. However, at position between 80º and 100º the flow is already developed, and no change in velocity profile is verified until the end of the curve. Up to 80º, for *Re*=532 the flow develops in the same way as for *Re*=486. After 100º the velocity profile shows that the maximum velocity moves back toward the centre of the channel, which confirms the early development of the additional vortices near the outer wall, and the flow does not reach a fully developed regime as it progresses along the curve. For *Re*=583 the flow development is approximately the same up to 60º, but then the development of the additional pair of vortices occurs at an earlier position (80º), and downstream of 140º the maximum velocity peak is located near the centre of the channel. Once again, the curved channel length (a 180º curve that is $L = \pi R$) is not sufficient for the flow to develop completely before exiting through the outlet channel.

Now, comparing results with those obtained by Bara *et al* [3], it can be seen in Figure 4 that they are not completely in agreement. At *Re*=486 (Figure 4 a)) our results were practically the same as those of Bara *et al* [3]. This is also verified at *Re*=532 (Figure 4 b)) but only up to 140º. At 160º and 180º a slight difference is observed and a better agreement is obtained when our predictions use a somewhat higher Reynolds number of *Re*=556. At *Re*=583 the discrepancy between results becomes larger and is observed upstream of that for *Re*=532. At θ=100º and for higher angles there is a better match between our predictions and those of Bara *et al* [3] if the Reynolds number is increased to *Re*=600.

Conclusions

The purpose of this work was to verify the major characteristics of an incompressible Newtonian fluid flow in a curved duct of square cross section, already reported by many authors [1-7], as an introduction to a deeper investigation of this kind of flows in the future. Thus, the same conditions assumed by Bara *et al* [3] were also considered here.

It was verified that at 90º only for the higher *Re*= of 580 signs of an additional pair of counter-rotating vortices appear near the outer wall.

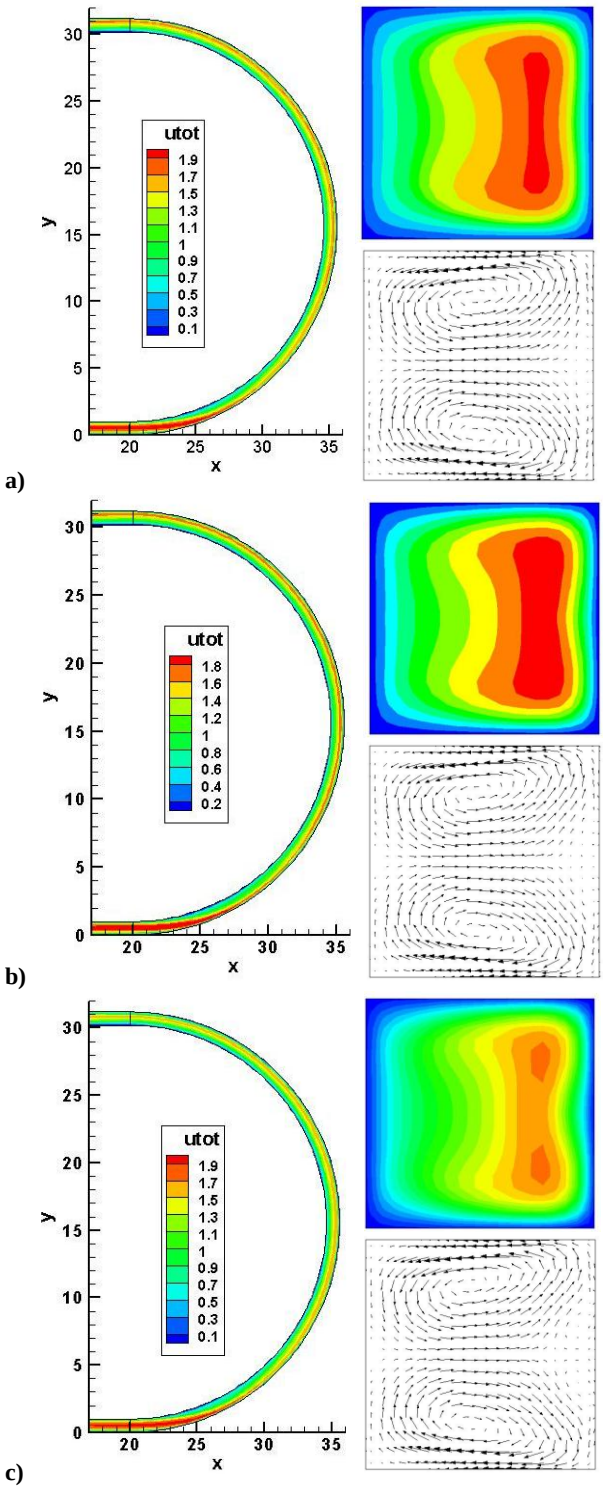

Figure 3 – Counters of axial velocity in the central plane of the channel (left) and the cross-section (right top) and velocity vectors in the cross-section (right bottom) at position of 90º for: **a)** *Re*=486 (*Dn*=125), **b)** *Re*=532 (*Dn*=137) and **c)** *Re*=583 (*Dn*=150).

In general, the evolution of velocity profiles in the channel is very similar for the different *Re*. At the beginning of the curved channel the maximum velocity is rapidly shifted towards the outer wall; further downstream the maximum velocity peak decreases and starts to move

back to the centre of the channel, because the secondary flow sets in and there is a tendency for the flow to recover a more fully profile shape. For *Re*=482 the flow is fully developed before the maximum velocity reaches the centre of the channel, and the flow is characterised by a secondary flow consisting of one pair of counter-rotating vortices. On the other hand, for *Re*=583 the maximum velocity (which was located near the wall at the initial stages of the curve) almost reaches the centre of the channel due to the appearance of an additional pair of vortices.

The velocity profiles at the central plane of the channel were compared with those presented by Bara *et al* [3]. Although good agreement was found for *Re*=480, the same was not verified for higher *Re*. At *Re*=532, the disparity between the results is small and is only observed at the end of the curve. However, for *Re*=580 the differences tend to increase and occur earlier in the flow. In order to match the results to those of Bara *et al* [3] it was necessary to use higher values of *Re* for the *Re*=532 and 583 cases of Bara *et al* [3].

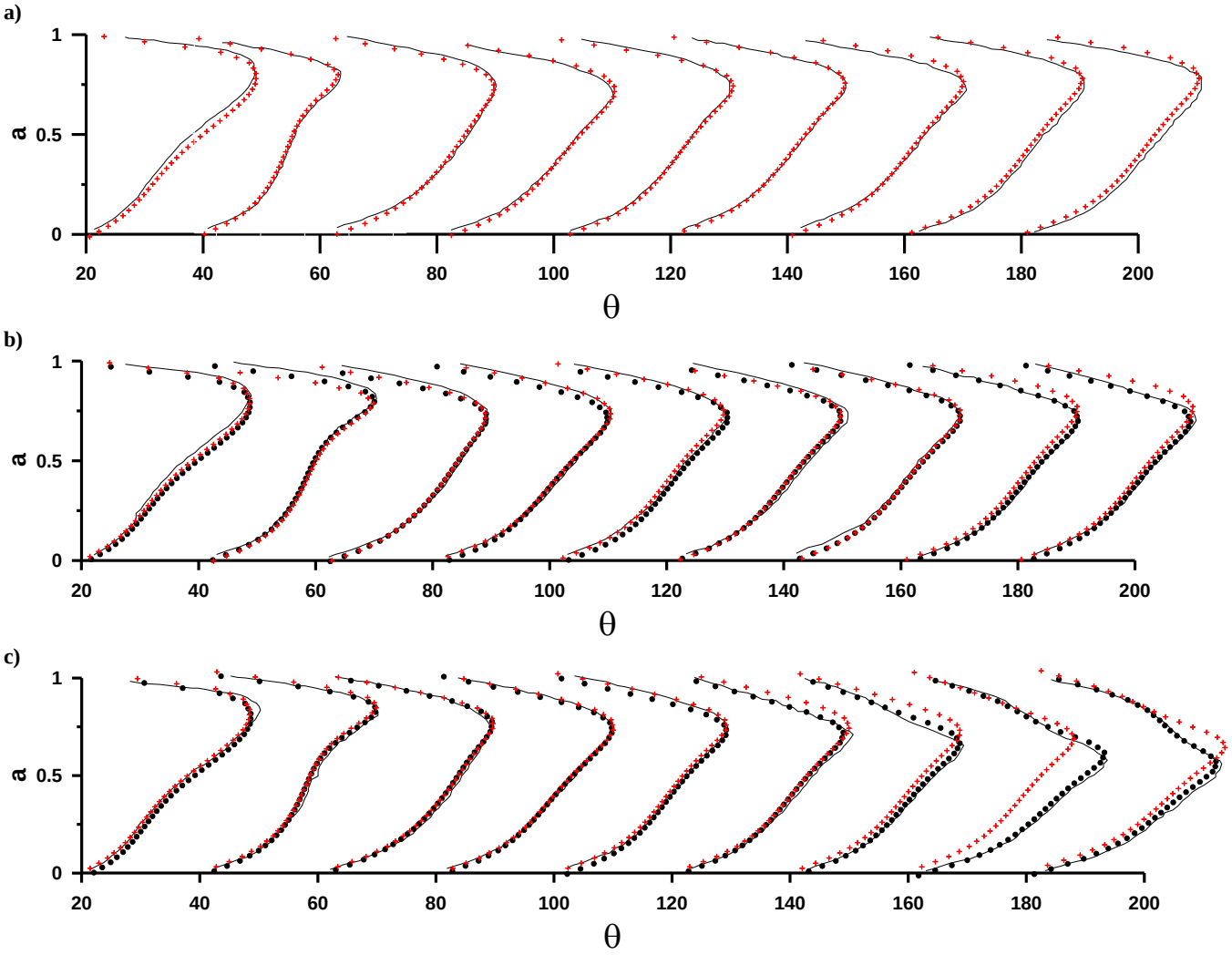

Figure 4 – Comparison of the predicted velocity profiles at the central plane of the channel for: **a)** Re=486 (+); **b)** Re=532 (+) and 556 (●); **c)** Re= 583 (+) and 600 (●), against the results of Bara *et al* [3] (lines) for *Re*= 486 (**a)**), 532 (**b)**) and 583 (**c)**).

References

1. Vashisth, S., Kumar, V., Nigam, K.D.P., Ind. Eng. Chem. Res., 47, 3291, 2008.
2. Berger, S.A., Talbot, L., Yao, L.-S., Ann. Rev. Fluid Mech, 15, 461, 1983.
3. Bara, B., Nandakumar, K., Masliyah, J.H., J. Fluid Mech., 244, 339, 1992.
4. Mees, P.A.J., Nandakumar, K., Masliyah, J.H., J. Fluid Mech., 314, 227, 1996.
5. Winters, K.H., J. Fluid Mech., 180, 343, 1987.
6. Soh, W.Y., J. Fluid Mech., 188, 337, 1988.
7. Helin, L., Thais, L., Mompean, G., J. Non-Newtonian Fluid Mech, 156, 84, 2009.

Acknowledgements

The authors acknowledge Fundação para a Ciência e Tecnologia for the financial support under the project PTDC/EME-MFE/70186/2006.